

# Quantum Interference of Identical Photons from Remote Quantum Dots

Liang Zhai,<sup>1,\*</sup> Giang N. Nguyen,<sup>1</sup> Clemens Spinnler,<sup>1</sup> Julian Ritzmann,<sup>2</sup> Matthias C. Löbl,<sup>1</sup> Andreas D. Wieck,<sup>2</sup> Arne Ludwig,<sup>2</sup> Alisa Javadi,<sup>1</sup> and Richard J. Warburton<sup>1</sup>

<sup>1</sup>*Department of Physics, University of Basel, Klingelbergstrasse 82, CH-4056 Basel, Switzerland*

<sup>2</sup>*Lehrstuhl für Angewandte Festkörperphysik, Ruhr-Universität Bochum, DE-44780 Bochum, Germany*

Photonic quantum technology provides a viable route to quantum communication<sup>1,2</sup>, quantum simulation<sup>3</sup>, and quantum information processing<sup>4</sup>. Recent progress has seen the realisation of boson sampling using 20 single-photons<sup>3</sup> and quantum key distribution over hundreds of kilometres<sup>2</sup>. Scaling the complexity requires photonic architectures containing a large number of single photons, multiple photon-sources and photon-counters. Semiconductor quantum dots are bright and fast sources of coherent single-photons<sup>5–9</sup>. For applications, a significant roadblock is the poor quantum coherence upon interfering single photons created by independent quantum dots<sup>10,11</sup>. Here, we demonstrate two-photon interference with near-unity visibility using photons from remote quantum dots. Exploiting the quantum interference, we demonstrate a photonic controlled-not circuit and a high-fidelity entanglement between photons of different origins. Our results provide a long-awaited solution to the challenge of creating coherent single-photons in a scalable way. In the near future, they point to a demonstration of quantum advantage using quantum-dot single photons<sup>8</sup> and an implementation of device-independent quantum key distribution<sup>2</sup>.

From large-scale quantum simulations<sup>3</sup> to multi-user quantum networks<sup>12</sup>, scaling of photonic technologies requires a large number of indistinguishable photons. At present, single-photon sources meeting these needs simply do not exist. While current proof-of-principle demonstrations of photonic quantum applications rely mostly on parametric down-conversion sources<sup>4,13,14</sup>, the adoption of solid-state-based deterministic sources is a clear trend<sup>5–9,15,16</sup>: semiconductor quantum dots (QDs) are on-demand emitters of single photons with a significantly higher efficiency and photon generation-rate than down-conversion sources<sup>6,9</sup>. In addition, QDs can be easily integrated into various nanostructures<sup>7,8,17</sup>. For single-photon generation, these advantages make QD-based sources arguably the best choice<sup>6,9</sup>. However, to create a large number of photons, the prevalent approach – active demultiplexing from a single QD<sup>3</sup> – is not optimal. It introduces additional losses and leads to a large resource overhead, limiting the maximal number of photons.

A more advantageous approach is to create indistinguishable photons simultaneously from multiple QDs. This method facilitates scaling up to higher photon numbers without sacrificing efficiency. However, putting this idea into practice has been a challenge for many years<sup>10,11,18,19</sup>. So far, the highest visibility on interfering photons created by two separate QDs is limited to 51%<sup>10</sup>. It is non-trivial to match the exact frequencies and radiative decay rates of the two QDs; yet, an exact match does not guarantee success. The underlying reason why this approach is so challenging is that quantum interference is sensitive to the total noise in two uncorrelated solid-state environments. Fast noise processes (upper-level dephasing) and slow noise processes (spectral fluctuations) over an enormous bandwidth all contribute. Suppressing the noise in the solid-state to a very low level is an essential albeit difficult task<sup>20</sup>. Despite the challenges, establishing high-visibility interference of photons from separate single-photon sources is a primary task for com-

plex quantum-photonic protocols – device-independent quantum key distribution (QKD)<sup>2</sup> and modular quantum information processing both hinge on it.

A breakthrough is presented in this work. By interfacing the photons created by two separate QDs in distant cryostats, we report an unprecedentedly high two-photon interference visibility of  $V = 93\%$ . The key is the employment of gated GaAs QDs. This system exhibits an ultra-low level of noise: exciton dephasing is slow compared to the radiative rate; spectral fluctuations are weak compared to the spectral linewidth. We exploit the photon-photon interference to introduce entangling capabilities to the remote solid-state systems [Figure 1(a)]. We demonstrate a controlled-not (CNOT) gate – the fundamental two-qubit logic in quantum algorithms – between two independently generated streams of photons. Utilising the CNOT operation, an entangled two-photon state is created: in the entangled pair, one photon is created by one semiconductor chip, the other photon is created by a separate chip far apart. Our results suggest that the GaAs QD platform represents a versatile launchpad for scalable photonic technologies.

Our semiconductor system consists of GaAs QDs in an  $\text{Al}_{0.33}\text{Ga}_{0.67}\text{As}$  matrix grown by local droplet etching<sup>21</sup> [Figure 1(a)]. These QDs create single photons at deep-red wavelengths (750 – 800 nm), a very convenient spectral band: low-loss optical fibres, semiconductor lasers and highly efficient single-photon detectors are readily available. On account of ultra-pure materials and a specially designed *n-i-p* diode<sup>22</sup>, the noise in the system is very low. Close-to-lifetime-limited spectral linewidths and elimination of blinking<sup>22</sup> are observed on the majority of QDs in our heterostructure. Results on the negative trions ( $\text{X}^-$ ) of two typical QDs, QD1 and QD2, are presented. For both QDs, the linewidth is only marginally (below 10%) larger than the lifetime-limit.

For on-demand single-photon generation, we excite the QDs resonantly with short laser pulses (duration 6 ps). A

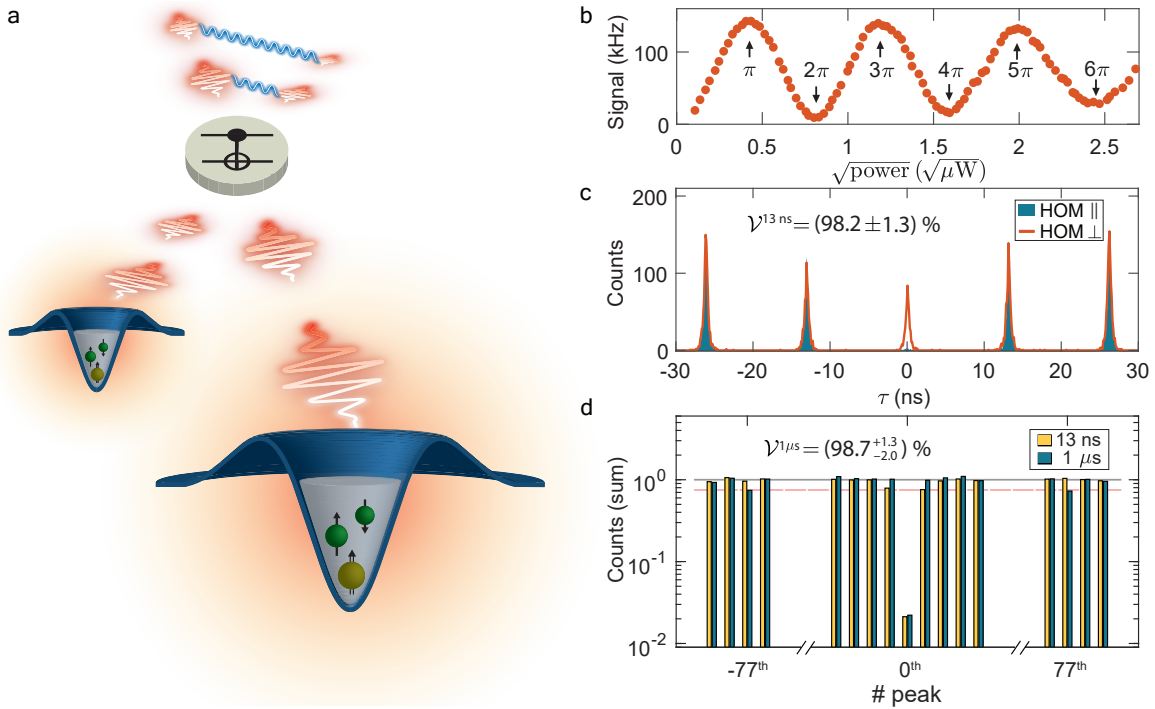


**FIG. 1. Coherent single photons from GaAs quantum dots at a wavelength of 780 nm.** (a) A schematic view of an entangling gate between photons from two separate GaAs QDs. Each QD is excited independently (creating two electrons and one hole, the  $X^-$ ) and generates a stream of single photons. Two streams of photons are entangled by an optical controlled-NOT (CNOT) circuit. (b) Resonance fluorescence from an individual QD (QD2,  $X^-$ ) reveals Rabi oscillations. A  $\pi$ -pulse power is chosen for all subsequent experiments. (c) Hong-Ou-Mandel (HOM) experiments on QD2  $X^-$  showing quantum interference of photons created 13 ns apart. (d) Two-photon interference for two different delays, 13 ns and 1  $\mu$ s. Each bar represents the total coincidence counts summing over one whole pulse period and is normalised at long delays. The coincidence probability is nearly identical for the two delays, while the side peaks are flat and close to one (grey line). The red line indicates the decrease to 75% due to classical interference.

22 GHz-bandwidth spectral filter is inserted in the collection to improve laser suppression and to remove the weak phonon sideband as well as the weak radiative Auger emission<sup>23</sup>. Figure 1(b) shows Rabi oscillations up to  $6\pi$ . The first Rabi cycle shows the highest contrast – at a Rabi power of  $2\pi$  the signal intensity drops to just  $\sim 6\%$  of that at  $\pi$ .

In the following experiments, a  $\pi$ -pulse power is used to ensure that the excited state population is maximised to near-unity before photon creation. The purity of the photons, as characterised by  $g^{(2)}(0)$  in a Hanbury Brown-Twiss measurement, is  $(99.0 \pm 0.1)\%$ . To probe the indistinguishability, we perform a HOM experiment: the single photons are sent into a Mach-Zehnder interferometer, where a photon travelling through the longer path overlaps on a symmetric beamsplitter with the  $\mathcal{N}^{\text{th}}$  subsequently emitted photon travelling through the shorter path. Figure 1(c) shows the HOM measurements on QD2  $X^-$  for  $\mathcal{N} = 1$ , i.e. the delay of the interferometer corresponds to one repetition pulse-period ( $\mathcal{D} = 13$  ns). By preparing the two photons in the same polarisation (co-polarisation) the central HOM peak vanishes due to quantum interference. On the contrary, the photons become distinguishable in cross-polarisation: the quan-

tum interference no longer takes place and the central peak appears. The raw HOM visibility, defined as the ratio of the central-peak intensity between co-polarised (HOM  $\parallel$ ) and cross-polarised (HOM  $\perp$ ) configurations, is  $\mathcal{V}_{\text{raw}}^{13\text{ns}} = (95.8 \pm 1.2)\%$ . The true HOM visibility for QD2 is  $\mathcal{V}^{13\text{ns}} = (98.2 \pm 1.3)\%$  on correcting<sup>24</sup> the raw HOM visibility for the finite  $g^{(2)}(0)$  and experimental imperfections. Here, we calculate  $\mathcal{V}$  by summing over the whole pulse period [the yellow bars in Fig. 1(d)]. This time bin ( $T_{\text{bin}} = 13$  ns) is significantly larger than the QD lifetime ( $1/\Gamma_2 = 256$  ps) and thus introduces no temporal post-selection. (Narrowing the time bin  $T_{\text{bin}}$  artificially increases the HOM visibility at the expense of efficiency.) For QD1, we achieve comparable results:  $g^{(2)}(0) = (1.3 \pm 0.2)\%$ , and  $\mathcal{V}^{13\text{ns}} = (97.8 \pm 1.8)\%$ .

The ambient environment of a QD can be static on a short time-scale such that it has little impact<sup>25</sup> on the coherence between consecutively emitted photons ( $\mathcal{N} = 1$ ). However, slowly varying noise, for instance spectral fluctuations, decrease the HOM visibility on longer time-scales<sup>26,27</sup>. By adding a 200-metre fibre to the HOM interferometer, we extend the delay to  $\mathcal{D} \sim 1 \mu\text{s}$ , overlapping the two photons separated by 77 pulse periods ( $\mathcal{N} = 77$ ). Coincidence events of 13 ns and 1  $\mu\text{s}$  sepa-

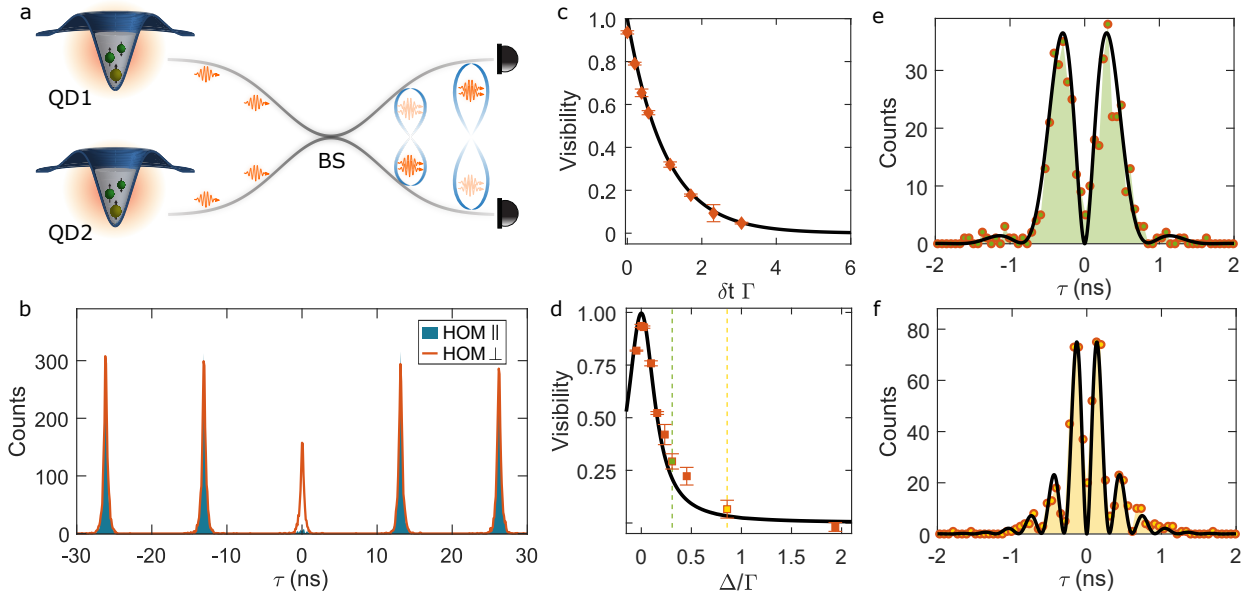


FIG. 2. **Two-photon interference from remote quantum dots.** (a) Schematic representation of the quantum interference between two remote GaAs QDs. Provided the photons are indistinguishable, they coalesce and exit the beamsplitter (BS) at the same port. (b) HOM interference from photons generated by two remote QDs. The vanishing central peak shows a raw HOM visibility of  $(90.9 \pm 0.8)\%$  and a true two-photon interference visibility of  $(93.0 \pm 0.8)\%$ . (c,d) Remote-QD HOM visibility as a function of normalised temporal delay  $\delta t$  and spectral detuning  $\Delta$  between the two QDs. (e,f) Pronounced quantum beats are revealed in the remote-QD HOM central peak when the QDs are slightly detuned in frequency. The green and yellow colours indicate the detuning in (d). The solid-lines in (c), (d), (e), and (f) show the quantum optical theory.

tion are compared in Fig. 1(d). We extract a raw HOM visibility for the  $1 \mu\text{s}$  case,  $\mathcal{V}_{\text{raw}}^{1\mu\text{s}} = (95.7 \pm 2.0)\%$  and  $\mathcal{V}^{1\mu\text{s}} = (98.7^{+1.3}_{-2.0})\%$ . (Similarly good results are achieved on QD1,  $\mathcal{V}^{1\mu\text{s}} = (99.0^{+1.0}_{-1.8})\%$ .) As for the  $13 \text{ ns}$  case, the  $1 \mu\text{s}$  HOM visibility remains near-unity. As far as the HOM is concerned, we deduce that the QD environment is static over a time-scale at least  $\sim 5 \times 10^3$  larger than the QD's lifetime.

For multi-qubit applications, the ultimate goal is to achieve two-photon interference from independent single-photon sources [Fig. 2(a)]. For QD-based sources, the challenge lies not only in matching emitters both spectrally and temporally but also in suppressing noise over a huge bandwidth. Exploiting the large Stark tuning, QD1 and QD2 are well-matched: their temporal overlap is  $\Gamma_1/\Gamma_2 = 96\%$ , while the spectral overlap is  $\Delta\nu_1/\Delta\nu_2 = 95\%$  (with  $\Delta\nu_{1,2}$  denoting the measured linewidths). QD1 and QD2 are located in two individual wafer pieces and are hosted in two cryostats separated by 20 metres (in fibre length). The environments of QD1 and QD2 are therefore completely uncorrelated. As such, the HOM interference of the photons created by two remote QDs is, to a certain extent, equivalent to the coalescence of two infinitely delayed photons ( $\mathcal{N} \rightarrow \infty$ ): the HOM visibility is sensitive to the noise in both semiconductor environments over an enormous bandwidth. Despite this sensitivity to environmental noise, the remote HOM visibility is profound,  $\mathcal{V}^{\text{remote}} = (93.0 \pm 0.8)\%$  [Fig. 2(b)]. The two QD environments, therefore, must

be near-perfectly static. Side peaks of the normalised HOM are perfectly flat, verifying that blinking is absent in both QD systems. The high visibility is not limited to only one pair of QDs: we repeat the experiments with another QD (QD3) in the QD2-cryostat. Between QD1 and QD3, a similar remote-QD HOM visibility of  $\mathcal{V}^{\text{remote}} = (92.7 \pm 1.6)\%$  is observed.

The remote-QD two-photon interference experiments are carried out under rigorous conditions: there is no Purcell enhancement of the radiative rate, no temporal post-selection, no narrow spectral filtering, and no active frequency stabilisation. Therefore, the record-high remote-HOM visibility is unambiguous evidence of the low noise-level in the system.

The low-noise in the semiconductor determines the remaining imperfections in the HOM visibilities. The fast noise-process is exciton dephasing at rate  $\Gamma^*$ . This process is likely to arise from phonon scattering<sup>25,27</sup>, resulting in a contribution to the homogeneous spectral linewidth of  $\Delta\nu_H = \Gamma^*/\pi$ . Random changes in the local environment of the QDs are responsible for the slow noise-process<sup>20</sup> – a spectral fluctuation. Assuming identical QDs and a Lorentzian probability distribution<sup>20</sup> for each QD (with frequency width  $\Delta\nu_H$ ) to describe the spectral fluctuations, the two-QD HOM visibility  $\mathcal{V}$  is given by:

$$\mathcal{V} = \frac{1}{1 + 2\pi(\Delta\nu_H + \Delta\nu_S) \cdot \tau_r},$$

where  $\tau_r$  is the radiative lifetime. This result demonstrates that a high  $\mathcal{V}$  is achieved only when both exciton dephasing and spectral fluctuations are suppressed. In the one-QD HOM experiment, the environment is static ( $\Delta\nu_S \rightarrow 0$ ) and the imperfection in  $\mathcal{V}$  determines the homogeneous broadening. We find  $\Gamma^* = 34 \pm 25$  MHz, equivalently  $\Delta\nu_H = 11 \pm 8$  MHz. In the remote two-QD HOM experiment,  $\mathcal{V}$  depends on both exciton dephasing and spectral fluctuations allowing  $\Delta\nu_S = 34 \pm 15$  MHz to be determined. The total single-QD linewidth predicted from this HOM-analysis,  $1/(2\pi\tau_r) + \Delta\nu_H + \Delta\nu_S$ , matches well with the measured linewidth. This analysis shows that together, the one-QD and two-QD HOM experiments enable the fast and slow noise-processes to be determined separately.

The high visibility in the two-photon interference of photons from different QDs is a benchmark for the application of the GaAs QD system in quantum photonics. The visibility is higher than that achieved in trapped ion<sup>28</sup> and cold atom<sup>29</sup> experiments where the major limitation is Doppler broadening. It is comparable to the value achieved with state-of-the-art down-conversion photon-pair sources<sup>14</sup> as well as with coherent scattering from solid-state emitters<sup>30</sup>. However, both down-conversion and coherent scattering operate in an intrinsically probabilistic manner where the photon generation rate is compromised in order to achieve high indistinguishability. The remote-QD visibility is also slightly higher than that achieved with remote nitrogen-vacancy centres<sup>31,32</sup> for which narrow time- and frequency-filters are required: both considerably decrease the impact of noise (spectral fluctuations) at the expense of a reduced efficiency. Overall, our system is presently the only one that allows high-visibility photon-photon quantum interference from multiple emitters with no trade-off in efficiency.

To map out the dependence of the remote-QD HOM visibility on the two-photon coalescence, we deliberately reduce the overlap either temporally or spectrally. In Fig. 2(c), the QD2 photons are delayed with respect to QD1 by  $\delta t$ . As  $\delta t$  increases, the remote-QD HOM visibility decreases exponentially, a consequence of the reduced overlap of the two wave-functions. This is in excellent agreement with theoretical expectations for exponentially-decaying wave-packets<sup>33</sup>. Exploiting the exquisite frequency control provided by the electrical gates, we explore also the dependence of the two-photon interference on the frequency detuning  $\Delta$  between the two QDs. The remote-QD HOM visibility follows a Lorentzian profile on detuning [Fig. 2(d)], again exactly as expected from theory. This configuration offers a further test of the photon coherence. When the two photons are slightly detuned in frequency, a quantum beat is expected in the time-dependence of the intensity correlation function<sup>33</sup>. These quantum beats are very clearly observed: Figure 2(d, e) show quantum beats in the central HOM peak for  $\Delta/\Gamma = 0.31$  and  $\Delta/\Gamma = 0.87$ , respectively. The oscillation period decreases as  $\Delta$  increases. These pronounced

quantum beats match nicely with theoretical predictions, and, from a different perspective, reflect the coherence of the photons created by the two remote QDs.

The highly indistinguishable photons from distant QDs enable the creation of a quantum logical unit, a controlled-not gate. The information can be encoded into the two separate streams of photons, and the CNOT unit allows the creation of entanglement between photons of different origins. The optical CNOT circuit can be realised by a combination of two half-wave plates (HWP) at 45° and three partially polarising beamsplitters<sup>15</sup> (PPBS), as depicted in Fig. 3(a). Single photons from the remote QDs are encoded as polarisation qubits:  $|H\rangle = |0\rangle$ ,  $|V\rangle = |1\rangle$ . Each 45° HWP acts as a Hadamard gate; the three PPBSs constitute a controlled-phase gate<sup>34</sup>. The controlled-phase gate relies on coincidence clicks on detectors in two opposite output arms. The central PPBS transmits  $H$ -polarised qubits  $T_H = 1$ , and partially reflects (transmits)  $V$ -polarised qubits  $R_V = 2/3$  ( $T_V = 1/3$ ). Upon simultaneous arrival at the PPBS, quantum interference between two indistinguishable photons provides a  $\pi$ -phase shift in the  $|VV\rangle$  amplitude<sup>34</sup>. The other two PPBSs are rotated by 90°, such that  $T_V = 1$  and  $T_H = 1/3$ , in order to compensate the imbalance between  $H$ - and  $V$ -polarised components in the output. Overall, the gate has a success probability of 1/9.

We evaluate the gate performance using the input-output relations in both the computational basis  $|H\rangle / |V\rangle$  and in the basis defined by the linear superpositions  $|\pm\rangle = 1/\sqrt{2}(|H\rangle \pm |V\rangle)$ . Ideally, in the  $|H\rangle / |V\rangle$  basis ( $ZZ$  basis in Pauli matrix language) the target qubit undergoes a flip when the control reads logical one. In the  $|+\rangle / |-\rangle$  basis ( $XX$  basis), the target qubit decides whether its control counterpart undergoes a flip. In the experiment, single photons from the remote QDs are carefully balanced to the same intensity at the two input arms where their polarisations prepare the input states. For every input state, the output state is mapped out using four simultaneous coincidence measurements in a quantum tomography setup. As in the HOM analysis, we integrate the coincidence events in the central peak over the whole pulse period. The corresponding truth tables are shown in Fig. 3(b, c). The fidelity of the CNOT operation is  $\mathcal{F}_{ZZ} = (88.90 \pm 5.34)\%$ , and  $\mathcal{F}_{XX} = (89.34 \pm 5.29)\%$ . We calculate the bound for the quantum process fidelity<sup>15</sup> of our CNOT gate based on  $\mathcal{F}_{ZZ} + \mathcal{F}_{XX} - 1 < \mathcal{F}_{\text{proc}} < \min(\mathcal{F}_{ZZ}, \mathcal{F}_{XX})$ , yielding  $(78.24 \pm 7.53)\% < \mathcal{F}_{\text{proc}} < (88.90 \pm 5.34)\%$ . The deviation from unity is mainly caused by imperfections of the optical elements and the slight deviation from the ideal indistinguishability of the remote QDs.

Finally, we demonstrate the ability to create maximally entangled states using the photonic qubits from remote QDs. This is the hallmark of the CNOT operation – by preparing the input state as  $|- \rangle_c |V\rangle_t$ , the Bell state  $|\Psi^-\rangle = \frac{1}{\sqrt{2}}(|HV\rangle - |VH\rangle)$  is produced. To characterise fully the produced state, quantum state to-

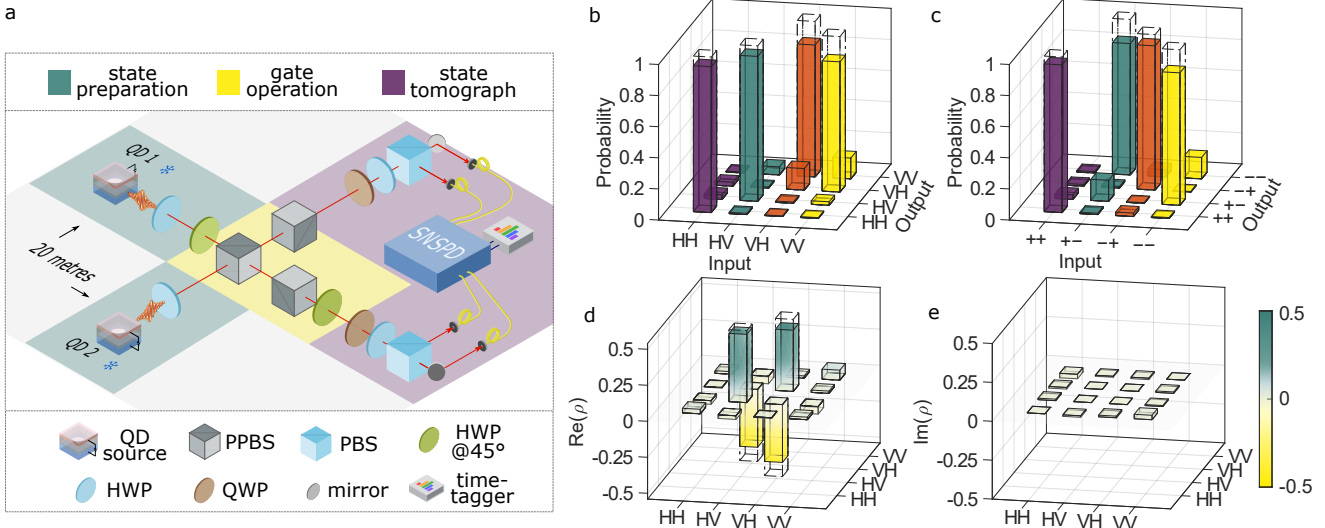


FIG. 3. **A quantum logic gate connecting photons from remote quantum dots.** (a) Sketch of the experimental setup for the CNOT gate based on two-photon interference between remote QDs. The photons from QD2 are used for the control qubit, and the photons from QD1 for the target qubit. After the gate operation (highlighted in yellow), the quantum state is projected by coincidence measurements. (b,c) The truth tables for  $|H\rangle / |V\rangle$  and  $|+\rangle / |-\rangle$  bases. The coincidence events are converted to probabilities by normalising to the respective input state. For each input state, we accumulate total coincidence counts of  $\sim 500$ . The empty dashed bars represent the ideal CNOT operation. (d,e) The real and imaginary parts of the density operator of state  $|\Psi^-\rangle$  created by the CNOT gate. The real parts of the measured density matrix are close to ideal (represented by the empty bars). In the imaginary parts, the intensities of all the bars are below 0.03.

mography is performed with a series of 36 coincidence measurements, followed by state reconstruction using a maximum-likelihood-estimation algorithm<sup>35</sup>. The real and imaginary parts of the reconstructed density matrix  $\rho$  are shown in Fig. 3(d, e). We obtain an entanglement fidelity of  $\mathcal{F}_{\Psi^-} = (85.02 \pm 0.97)\%$ , which exceeds the threshold of  $(2 + 3/\sqrt{2})/8 = 0.78$  for violating Bell inequalities<sup>34</sup>. To quantify the entanglement, we calculate the concurrence  $C = (74.67 \pm 1.93)\%$  and the linear entropy  $S_L = (34.04 \pm 1.94)\%$ . These values indicate a high level of entanglement and purity of the generated  $|\Psi^-\rangle$  state. Compared to CNOT gates constructed in a similar approach (but not using separate photon sources), the process fidelity of our remote-QD based CNOT gate, as well as the entanglement creation, has one of the best performances<sup>15,34,36</sup>.

In conclusion, we have demonstrated that GaAs QDs are interconnectable sources of indistinguishable single photons. Our work provides a feasible solution to the scaling bottleneck of photonic quantum technologies. The extraction efficiency of our system can be boosted by the Purcell effect upon coupling the QDs to a single optical mode via photonic engineering, e.g. on-chip photonic crystal waveguides<sup>7,8</sup>, open-microcavities<sup>9</sup> and micropillars<sup>6</sup>. The HOM visibility should also benefit from the reduced lifetime – the shortened lifetime leads to an increased visibility provided the low noise can be preserved (Eq. ). With the present noise level, a Purcell factor  $F_p \sim 10$  should result in one-QD and two-QD HOM visibilities of 99.6% and 99.0%, respec-

tively. From a quantum-information perspective, increasing the number of identical single-photons to  $\sim 50$  will lead to quantum advantage in a photonic boson sampling experiment<sup>8</sup>. This number of indistinguishable photons is within reach, for instance using two or three low-noise GaAs QD sources together with current photonic technologies<sup>3</sup>. From a quantum communication perspective, highly indistinguishable photons forge a coherent link between remote QDs, a route to the realisation of device-independent QKD. Moreover, the GaAs QDs can be brought into exact resonance with the rubidium transitions, allowing coherent QD single-photons to be stored in a rubidium-based quantum memory<sup>37</sup>.

## ACKNOWLEDGEMENTS

We thank Peter Lodahl and Philipp Treutlein for stimulating discussions. The work was supported by NCCR QSIT and SNF Project No. 200020\_175748. LZ, GNN, AJ received funding from the European Union's Horizon 2020 Research and Innovation Programme under the Marie Skłodowska-Curie grant agreement No. 721394 (4PHOTON), No. 861097 (QUDOT-TECH), and No. 840453 (HiFig), respectively. JR, ADW and AL acknowledge financial support from the grants DFH/UFA CDFA05-06, DFG TRR160, DFG project 383065199, and BMBF Q.Link.X 16KIS0867.

## CONTRIBUTIONS

LZ, GNN, CS, AJ carried out the experiments. JR, LZ, MCL, ADW, AL designed and grew the sample. CS, GNN, LZ fabricated the sample. LZ, GNN, CS, AJ, MCL, RJW analysed the data. LZ, GNN, CS, RJW wrote the manuscript with input from all the authors.

\* liang.zhai@unibas.ch

- <sup>1</sup> Tanzilli, S. *et al.* A photonic quantum information interface. *Nature* **437**, 116–120 (2005).
- <sup>2</sup> Yin, H.-L. *et al.* Measurement-device-independent quantum key distribution over a 404 km optical fiber. *Phys. Rev. Lett.* **117**, 190501 (2016).
- <sup>3</sup> Wang, H. *et al.* Boson sampling with 20 input photons and a 60-mode interferometer in a  $10^{14}$ -dimensional Hilbert space. *Phys. Rev. Lett.* **123**, 250503 (2019).
- <sup>4</sup> Qiang, X. *et al.* Large-scale silicon quantum photonics implementing arbitrary two-qubit processing. *Nat. photonics* **12**, 534–539 (2018).
- <sup>5</sup> Strauf, S. *et al.* High-frequency single-photon source with polarization control. *Nat. photonics* **1**, 704–708 (2007).
- <sup>6</sup> Senellart, P., Solomon, G. & White, A. High-performance semiconductor quantum-dot single-photon sources. *Nat. Nanotechnol.* **12**, 1026–1039 (2017).
- <sup>7</sup> Liu, F. *et al.* High Purcell factor generation of indistinguishable on-chip single photons. *Nat. Nanotechnol.* **13**, 835–840 (2018).
- <sup>8</sup> Uppu, R., Midolo, L., Zhou, X., Carolan, J. & Lodahl, P. Single-photon quantum hardware: towards scalable photonic quantum technology with a quantum advantage (2021). arXiv:2103.01110.
- <sup>9</sup> Tomm, N. *et al.* A bright and fast source of coherent single photons. *Nat. Nanotechnol.* **16**, 399–403 (2021).
- <sup>10</sup> Reindl, M. *et al.* Phonon-assisted two-photon interference from remote quantum emitters. *Nano Lett.* **17**, 4090–4095 (2017).
- <sup>11</sup> Weber, J. H. *et al.* Two-photon interference in the telecom C-band after frequency conversion of photons from remote quantum emitters. *Nat. Nanotechnol.* **14**, 23–26 (2018).
- <sup>12</sup> Sangouard, N., Simon, C., de Riedmatten, H. & Gisin, N. Quantum repeaters based on atomic ensembles and linear optics. *Rev. Mod. Phys.* **83**, 33–80 (2011).
- <sup>13</sup> Adcock, J. C., Vigliar, C., Santagati, R., Silverstone, J. W. & Thompson, M. G. Programmable four-photon graph states on a silicon chip. *Nat. Commun.* **10**, 3528 (2019).
- <sup>14</sup> Llewellyn, D. *et al.* Chip-to-chip quantum teleportation and multi-photon entanglement in silicon. *Nat. Phys.* **16**, 148–153 (2020).
- <sup>15</sup> He, Y.-M. *et al.* On-demand semiconductor single-photon source with near-unity indistinguishability. *Nat. Nanotechnol.* **8**, 213–217 (2013).
- <sup>16</sup> Basset, F. B. *et al.* Quantum key distribution with entangled photons generated on demand by a quantum dot. *Sci. Adv.* **7**, eabe6379 (2021).
- <sup>17</sup> Grim, J. Q. *et al.* Scalable in operando strain tuning in nanophotonic waveguides enabling three-quantum-dot superradiance. *Nat. Mater.* **18**, 963–969 (2019).
- <sup>18</sup> Zopf, M. *et al.* Frequency feedback for two-photon interference from separate quantum dots. *Phys. Rev. B* **98**, 161302 (2018).
- <sup>19</sup> Giesz, V. *et al.* Cavity-enhanced two-photon interference using remote quantum dot sources. *Phys. Rev. B* **92**, 161302 (2015).
- <sup>20</sup> Kuhlmann, A. V. *et al.* Charge noise and spin noise in a semiconductor quantum device. *Nat. Phys.* **9**, 570–575 (2013).
- <sup>21</sup> Zhai, L. *et al.* Large-range frequency tuning of a narrow-linewidth quantum emitter. *Appl. Phys. Lett.* **117**, 083106 (2020).
- <sup>22</sup> Zhai, L. *et al.* Low-noise GaAs quantum dots for quantum photonics. *Nat. Commun.* **11**, 4745 (2020).
- <sup>23</sup> Löbl, M. C. *et al.* Radiative Auger process in the single-photon limit. *Nat. Nanotechnol.* **15**, 558–562 (2020).
- <sup>24</sup> Santori, C., Fattal, D., Vučković, J., Solomon, G. S. & Yamamoto, Y. Indistinguishable photons from a single-photon device. *Nature* **419**, 594–597 (2002).
- <sup>25</sup> Schöll, E. *et al.* Resonance fluorescence of GaAs quantum dots with near-unity photon indistinguishability. *Nano Lett.* **19**, 2404–2410 (2019).
- <sup>26</sup> Wang, H. *et al.* Near-Transform-limited single photons from an efficient solid-state quantum emitter. *Phys. Rev. Lett.* **116**, 213601 (2016).
- <sup>27</sup> Thoma, A. *et al.* Exploring dephasing of a solid-state quantum emitter via time- and temperature-dependent Hong-Ou-Mandel experiments. *Phys. Rev. Lett.* **116**, 033601 (2016).
- <sup>28</sup> Maunz, P. *et al.* Quantum interference of photon pairs from two remote trapped atomic ions. *Nat. Phys.* **3**, 538–541 (2007).
- <sup>29</sup> Beugnon, J. *et al.* Quantum interference between two single photons emitted by independently trapped atoms. *Nature* **440**, 779–782 (2006).
- <sup>30</sup> Stockill, R. *et al.* Phase-tuned entangled state generation between distant spin qubits. *Phys. Rev. Lett.* **119**, 010503 (2017).
- <sup>31</sup> Bernien, H. *et al.* Heralded entanglement between solid-state qubits separated by three metres. *Nature* **497**, 86–90 (2013).
- <sup>32</sup> Humphreys, P. C. *et al.* Deterministic delivery of remote entanglement on a quantum network. *Nature* **558**, 268–273 (2018).
- <sup>33</sup> Kambs, B. & Becher, C. Limitations on the indistinguishability of photons from remote solid state sources. *New J. Phys.* **20**, 115003 (2018).
- <sup>34</sup> Kiesel, N., Schmid, C., Weber, U., Ursin, R. & Weinfurter, H. Linear optics controlled-phase gate made simple. *Phys. Rev. Lett.* **95**, 210505 (2005).
- <sup>35</sup> James, D. F. V., Kwiat, P. G., Munro, W. J. & White, A. G. Measurement of qubits. *Phys. Rev. A* **64**, 052312 (2001).

<sup>36</sup> Langford, N. K. *et al.* Demonstration of a simple entangling optical gate and its use in Bell-state analysis. *Phys. Rev. Lett.* **95**, 210504 (2005).

<sup>37</sup> Wolters, J. *et al.* Simple atomic quantum memory suitable for semiconductor quantum dot single photons. *Phys. Rev. Lett.* **119**, 060502 (2017).